Journal of Wind Engineering & Industrial Aerodynamics 222 (2022) 104919

Contents lists available at ScienceDirect

Journal of Wind Engineering & Industrial Aerodynamics

journal homepage: www.elsevier.com/locate/jweia

Numerical study of tornado-induced unsteady crosswind response of railway vehicle using multibody dynamic simulations

Dongqin Zhang [a], Takeshi Ishihara [b,*]

[a] School of Civil and Environmental Engineering, Harbin Institute of Technology, Shenzhen, China
[b] Department of Civil Engineering, School of Engineering, The University of Tokyo, Tokyo, Japan

ARTICLE INFO

Keywords:
Railway vehicle
Multibody dynamic simulations
Tornado winds
Uetsu line railway accident
Dynamic amplification factor

ABSTRACT

The tornado-induced unsteady crosswind responses of railway vehicles are investigated by using multibody dynamic simulations. Firstly, a tornado-induced aerodynamic force model is proposed by using the equivalent wind force method and the quasi-steady theory and validated by the experimental data. The Uetsu line railway accident caused by tornado winds on December 25, 2005 is then investigated by the proposed tornado-induced aerodynamic force model and the multi-body dynamic simulation. The predicted accident scenes show favorably agreement with those obtained from the accident survey when the maximum tangential velocity of tornado is around 41 m/s and the core radius is 30m. Finally, the dynamic amplification factor (DAF) for railway vehicles in tornado winds is systematically studied and it increases as the passing time decreases. It is found that the DAF can be effectively suppressed as the damping parameters increase while it decreases slightly as the natural frequency increases. A simple method to predict the DAF is also proposed based on simulation results.

1. Introduction

In the last decades, railway accidents induced by crosswinds have been reported by Baker et al. (2009) and a great deal of research has been conducted to assess the crosswind stability of railway vehicles (Sesma et al., 2012; Olmos and Astiz, 2018; Montenegro et al., 2020, 2021; Heleno et al., 2021; Zhai et al., 2019). Wind tunnel tests (Cheli et al., 2010, 2013; Schober et al., 2010; Tomasini et al., 2014; Kikuchi and Suzuki, 2015; Noguchi et al., 2019) or CFD simulations (Premoli et al., 2016; Maleki et al., 2017; Niu et al., 2017; Zhang et al., 2018) was firstly carried out to measure aerodynamic coefficients of railway vehicles subjected to either uniform or turbulent winds, and the quasi-steady theory was generally used to calculate aerodynamic forces. Afterwards, the quasi-static analysis or multi-body dynamic simulations was conducted to predict the crosswind responses of railway vehicles (EN 14067-6, 2010). Furthermore, aerodynamic forces and the dynamic response of railway vehicles in unsteady winds have also been studied.

Although tornadoes are low-occurrence hazards, it may threaten the operational safety of railway vehicles and cause severe damages. In fact, it was suspected that several railway accidents in Japan were induced by tornado winds, such as the Touzai line, the Uetsu line and the Nippo line railway accidents (Suzuki and Okura, 2016). A freight train was also attacked by a tornado and turned over when it passed through Illinois on January 8, 2008 (Bourriez et al., 2019). Therefore, it is necessary to evaluate tornado-induced aerodynamic forces and the corresponding dynamic response to make sure the operational safety of railway vehicles, especially in the high incidence area of tornadoes.

Recently, tornado-induced aerodynamic forces acting on railway vehicles have been investigated. Experiments including moving vehicle models passing through the tornado simulator (Bourriez et al., 2019; Suzuki and Okura, 2016) and stationary high-speed train models in the tornado simulator (Cao et al., 2019) were carried out, respectively. A moving high-speed train passes through a tornado simulator was numerically studied by Xu et al. (2020) as well. Using the Morison equation, tornado-induced aerodynamic forces on a train were also predicted by Baker and Sterling (2018), but the results were not compared with the experiments. It indicates that validation of the proposed methods to evaluate tornado-induced aerodynamic forces acting on railway vehicles is still necessary.

Furthermore, the Uetsu line railway accident has been investigated by ARAIC (2008) using the quasi-static analysis (Hibino et al., 2010), in which aerodynamic coefficients were measured by wind tunnel tests. It concluded that the maximum tangential velocity of the tornado was larger than 40 m/s which exceeded the critical wind speed of the limited express train, so the railway accident occurred. However, the

* Corresponding author.
E-mail address: ishihara@bridge.t.u-tokyo.ac.jp (T. Ishihara).

https://doi.org/10.1016/j.jweia.2022.104919
Received 13 September 2021; Received in revised form 19 January 2022; Accepted 25 January 2022

Nomenclature

a	first exponent of Δt
A	side area of car body
b	decay factor of DAF
c	a function of c_t
c_t	ratio of translational velocity to the maximum tangential velocity of a tornado
$C_{L.To}$	lift force coefficient in tornado simulator
$C_{L.WT}$	lift force coefficient in wind tunnel
$C_{M.WT}$	rolling moment coefficient in wind tunnel
$C_{S.To}$	side force coefficient in tornado simulator
$C_{S.WT}$	side force coefficient in wind tunnel
D	wheel unloading ratio
DAF	dynamic amplification factor
$D_{dynamic}$	dynamic wheel unloading ratio
d_{pi}	lateral distance of the *No.i* power pole
$d_{TL.A}$	lateral displacement of the top left corner of car body at point A
$d_{TL.B}$	lateral displacement of the top left corner of car body at point B
D_{static}	static wheel unloading ratio
D_{ys}	horizontal damping parameter in second suspension
D_{zs}	vertical damping parameter in second suspension
f_n	natural frequency of railway vehicle
$F_L(t)$	lift force
$F_S(t)$	side force
H_0	height of car body
K_{ys}	horizontal stiffness in second suspension
K_{zs}	vertical stiffness in second suspension
L	distance between lifting and crashing positions
L_0	length of carriage
m_B	mass of car body
$M_R(t)$	rolling moment
r	radial distance from the tornado center
R_{Max}	core radius
t	time
$v_a(t)$	relative wind speed to the train
$v_c(t)$	the temporal wind speed at the vehicle center
V	tangential velocity distributed in special domain
$V_{Max.S}$	maximum tangential velocity of a stationary tornado
$V_{Max.T}$	maximum tangential velocity of a moving tornado
V_T	translational velocity of tornado
V_{tr}	train speed
z	height from ground

Greek symbols

β	angle of attack for the relative wind speed
β_w	angle of attack for wind
Δt	passing time
ζ	total equivalent damping ratio
ζ_l	horizontal equivalent damping ratio
ζ_v	vertical equivalent damping ratio
ρ	air density
φ	translational direction of tornado

quasi-static analysis may underestimate the dynamic response of train in tornado winds caused by the short-rise-time gust (Ishihara et al., 2021). Moreover, critical wind curves were obtained when the wheel unloading ratio reached 100% and it implied the overturning of the limited express train happened when the wheels on the windward side lifted up. This criterion is rational to calculate the critical wind curve when a certain proportion of wheel unloading occurs since it preserves the safety margin for an operational railway vehicle, while it is not accurate to investigate the railway accident. It was pointed out that the railway vehicle would not turn over even if the wheel unloading ratio reached 100% by experiments (Hibino et al., 2013b). As for the vehicle, it was believed that the vehicle would ultimately roll over when the lateral displacement of the center of gravity exceeded the wheel (Chen and Chen, 2010). They imply that it is conservative to evaluate the overturning of railway vehicle by using wheel unloading ratio. In order to accurately investigate the railway accident, it is necessary to study vehicle dynamics by multi-body simulations and to evaluate the lateral displacement of the center of gravity of car body exceeding the wheel on the leeward side instead of the conventional critical wind curves for the overturning.

Moreover, numerical simulations and experiments have been carried out to study the dynamic responses of railway vehicles subjected to unsteady winds, such as the Chinese hat gust wind (Sesma et al., 2012; You et al., 2018; Neto et al., 2021), tunnel exit winds (Hibino et al., 2013a; Thomas et al., 2010; Ishihara et al., 2021), and abrupt winds induced by the local terrain (Liu et al., 2018, 2019, 2020). They showed that dynamic responses of railway vehicles under short-rise-time gust were extensively larger than those in steady winds even if the maximum wind speed was the same. Ishihara et al. (2021) proposed the dynamic amplification factor (DAF) to quantitatively investigate the dynamic amplification effect of the unsteady crosswind response caused by the tunnel exit wind, however, the DAF for railway vehicles in tornado winds has not been studied.

In this study, a framework to investigate the dynamic response of railway vehicles in tornado winds is proposed to investigate the train stability induced by tornado winds. The tornado-induced unsteady crosswind response of railway vehicles is investigated by using multi-body dynamic simulations and a dynamic amplification factor (DAF) for railway vehicle in tornado winds is proposed to evaluate the vehicle dynamics. A sensitivity study on the dynamic wheel unloading ratio is also performed considering the effects of the core radius, train speed, maximum tangential velocity and ratio of translational velocity to maximum tangential velocity. The dynamic wheel unloading ratios predicted by the proposed formula are compared with those from the multi-body dynamic simulations. Numerical models are introduced, including tornado-induced aerodynamic forces, railway vehicle models, and the Uetsu line railway accident in section 2. Tornado-induced aerodynamic forces are then investigated and validated by the laboratorial experiments. The Uetsu line railway accident is analyzed in detail using multibody dynamic simulations, and a fomula to predict the DAF for railway vehicles in tornado winds is proposed in section 3. Conclusions are summarized in section 4.

2. Numerical models

Tornado wind models and tornado-induced aerodynamic forces are interpreted in section 2.1. Railway vehicle models and investigation of the Uetsu line railway accident are then described in section 2.2 and section 2.3, respectively.

2.1. Tornado-induced aerodynamic forces

A schematic of a tornado hitting a railway vehicle is shown in Fig. 1. It is assumed that the tornado translates along y axis, while the railway vehicle runs along x axis. The profile of tangential velocity is also drawn in Fig. 1.

The analytical and empirical tornado models have been summarized (Gillmeier et al., 2018; Kim and Matsui, 2017). The Rankine combined

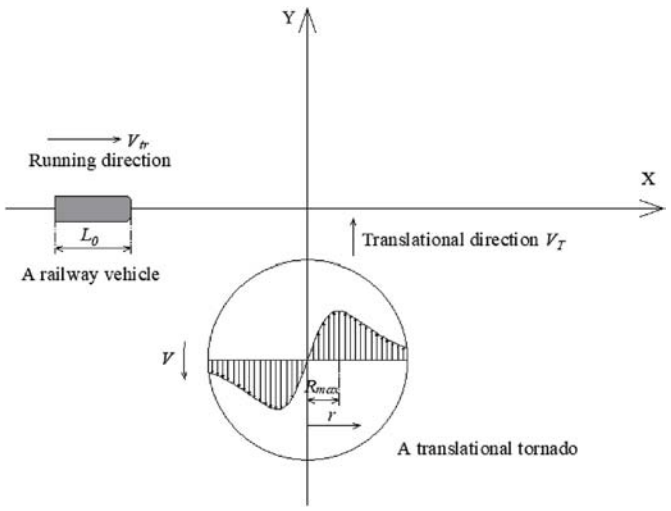

Fig. 1. A schematic of a tornado hitting a railway vehicle.

vortex (Rankine, 1882) separates the flow into two regions in which the tangential velocity increases linearly with the radial distance in the inner region and it is inversely proportional to the radial distance in the outer region. The Rankine combined vortex is the simplest tornado model, but the tangential velocity is not smooth at the core radius. The Burgers-Rott model (Burgers, 1948; Rott, 1958) is also widely used and the tangential velocity is expressed as Eq. (1).

$$V = \frac{V_{Max.S}}{0.72}\frac{R_{Max}}{r}\left\{1 - exp\left[-1.26\left(\frac{r}{R_{Max}}\right)^2\right]\right\} \tag{1}$$

where r refers to the radial distance from the tornado center and R_{Max} is the core radius as shown in Fig. 1. $V_{Max.S}$ is the maximum tangential velocity of the stationary tornado.

In order to calculate the wind field in a moving tornado, the translational velocity V_T is predicted by the statistical model (ANS, 1983) as shown in Eq. (2) and it is directly added to the stationary tornado wind field as expressed in Eq. (3).

$$V_T = c_t V_{Max.T},\ V_{Max.T} = V_{Max.S} + V_T \tag{2}$$

$$V = \frac{V_{Max.S}}{0.72}\frac{R_{Max}}{r}\left\{1 - exp\left[-1.26\left(\frac{r}{R_{Max}}\right)^2\right]\right\} + V_T \tag{3}$$

where $V_{Max.T}$ is the maximum tangential velocity of a moving tornado, c_t is a constant value and is assumed to be 0.15 in Japan (NRA, 2013).

The spatial distribution of wind speed acting on the vehicle changes extensively as the railway vehicle is attacked by a tornado. Ishihara et al. (2021) proposed a method to transform the spatial distribution of wind speed acting on the railway vehicle to the equivalent wind speed at the vehicle center and validated it using the wind tunnel test. In this study, tornado-induced aerodynamic forces are evaluated by the quasi-steady theory after the temporal wind speed at the railway vehicle center is low-pass filtered by the equivalent wind force method. The low-pass filter is expressed as:

$$v_c = \sqrt{\frac{\int_{\left(V_{tr}t-\frac{L_0}{2}\right)}^{\left(V_{tr}t+\frac{L_0}{2}\right)} V^2 dx}{L_0}} \tag{4}$$

where L_0, V_{tr} represent the length of car body and the train speed, respectively as illustrated in Fig. 1. V refers to the tangential wind speed of a tornado in spatial domain in Fig. 1. v_c represents the low-pass filtered temporal wind speed at the railway vehicle center as shown in Fig. 2(a).

The coordinate systems of wind direction and aerodynamic forces direction are shown in Fig. 2. The relative wind speed to railway vehicle $v_a(t)$ and the angle of attack of the relative wind speed $\beta(t)$ are calculated by using train speed V_{tr}, the low-pass filtered temporal wind speed $v_c(t)$ and the angle of attack for wind β_w, and are presented as:

$$v_a(t) = \sqrt{\left[V_{tr} + v_c(t)cos\beta_w\right]^2 + \left[v_c(t)sin\beta_w\right]^2} \tag{5}$$

$$\beta(t) = arctan\left[\frac{v_c(t)sin\beta_w}{V_{tr} + v_c(t)cos\beta_w}\right] \tag{6}$$

Aerodynamic forces and moments are calculated by the quasi-steady theory, where side force $F_S(t)$, lift force $F_L(t)$ and rolling moment $M_R(t)$ as shown in Fig. 2(b) are considered and expressed as:

$$F_S(t) = \frac{1}{2}\rho A C_{S.WT}(\beta(t))v_a^2(t) \tag{7}$$

$$F_L(t) = \frac{1}{2}\rho A C_{L.WT}(\beta(t))v_a^2(t) \tag{8}$$

$$M_R(t) = \frac{1}{2}\rho A C_{M.WT}(\beta(t))v_a^2(t)H_0 \tag{9}$$

where A, H_0 refer to side area and height of car body, respectively. $C_{S.WT}(\beta(t))$, $C_{L.WT}(\beta(t))$ and $C_{M.WT}(\beta(t))$ represent aerodynamic coefficients which are measured by wind tunnel tests in different wind directions.

2.2. Railway vehicle models

In general, the dynamic response of railway vehicle under crosswinds is predicted by quasi-static analysis or multibody dynamic simulations (EN 14067-6, 2010). As shown in Fig. 3, a quasi-static analysis which is proposed and validated by Hibino et al. (2010) is widely used to evaluate the critical wind speed of railway vehicle overturning under crosswinds in Japan. It is a 3DoFs and half car model with half of car body, one bogie and two wheelsets. Based on the principle of minimum potential energy and the static equilibrium equation, three degrees of freedom and wheel unloading ratio are calculated. In order to accurately

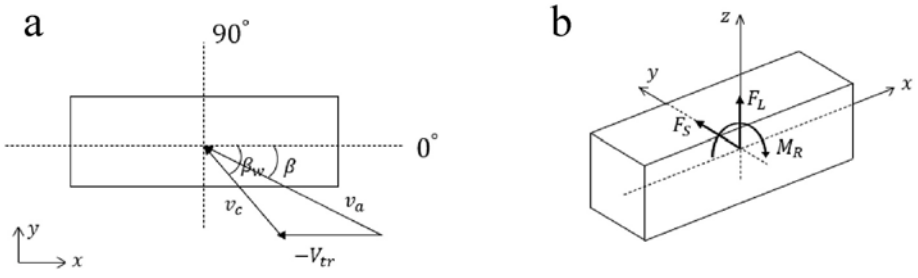

Fig. 2. Coordinate systems for: (a) wind direction; (b) aerodynamic forces direction.

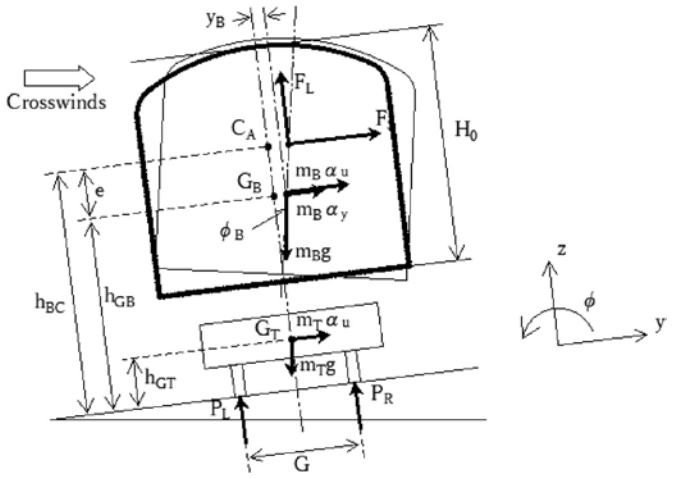

Fig. 3. A 3DoFs railway vehicle model.

predict the dynamic response of railway vehicle with different kinds of external excitations, a full vehicle model which consists of seven rigid components, namely, one car body, two bogies and four wheelsets is built by multibody dynamic simulations in Fig. 4. The whole vehicle model usually has 42 degrees of freedom, while the simplified vehicle model with 35DoFs (Zhai et al., 2013) or the refined vehicle model with 50DoFs (Sun et al., 2019) are also adopted to study the dynamic response of railway vehicles under crosswind. Subsequently, equations of motion of a railway vehicle are built and solved numerically by the commercial program SIMPACK (Dassault Systems, 2017).

Ishihara et al. (2021) explained the quasi-static analysis and multi-body dynamic simulations in detail and compared the dynamic response of railway vehicle under tunnel exit winds. It is found that wheel unloading ratio can be accurately predicted by the quasi-static analysis as the passing time is larger than 4s. However, the dynamic responses are underestimated by the quasi-static analysis if the passing time is smaller than 4s since the inertial terms and damping terms in equations of motion are neglected and they essentially affect the dynamic responses when the railway vehicle is attacked by the short-rise-time gust wind. Note that the critical passing time depends on the property of stiffness/damping and inertia of the model and should be evaluated for each vehicle.

2.3. Uetsu line railway accident

The Uetsu line railway accident occurred on December 25, 2005 in Japan and it was investigated by ARAIC (2008). It was suspected that the limited express train was attacked by tornado winds since the broken trees, the destroyed vinyl house and collapsed wind barriers along the tornado path was found, as shown in Fig. 5. It was also found that band destruction and tornado path were coincidence with the radar echo intensity data in Fig. 5. The basic parameters of the limited express train, including both structural parameters and aerodynamic coefficients measured by the wind tunnel test were reported in the railway accident investigation (ARAIC, 2008). The train speed was around 100 km/h when the accident happened. The translational velocity of the tornado was 25 m/s in accordance with the echo movement. The translational direction of tornado was predicted by the band destruction and it was approximately 64° as shown in Fig. 5. The core radius of the tornado is estimated as 30 m based on the guideline in Japan (NRA, 2013) and a destroyed snow barrier of around 21m. All parameters are summarized in Table 1.

The railway accident scene is described in Fig. 6 to understand the path of the tornado, destruction of power poles and the overturning position. It was supposed that the tornado translated on the right side of the house based on the wind tunnel test for investigating the destruction

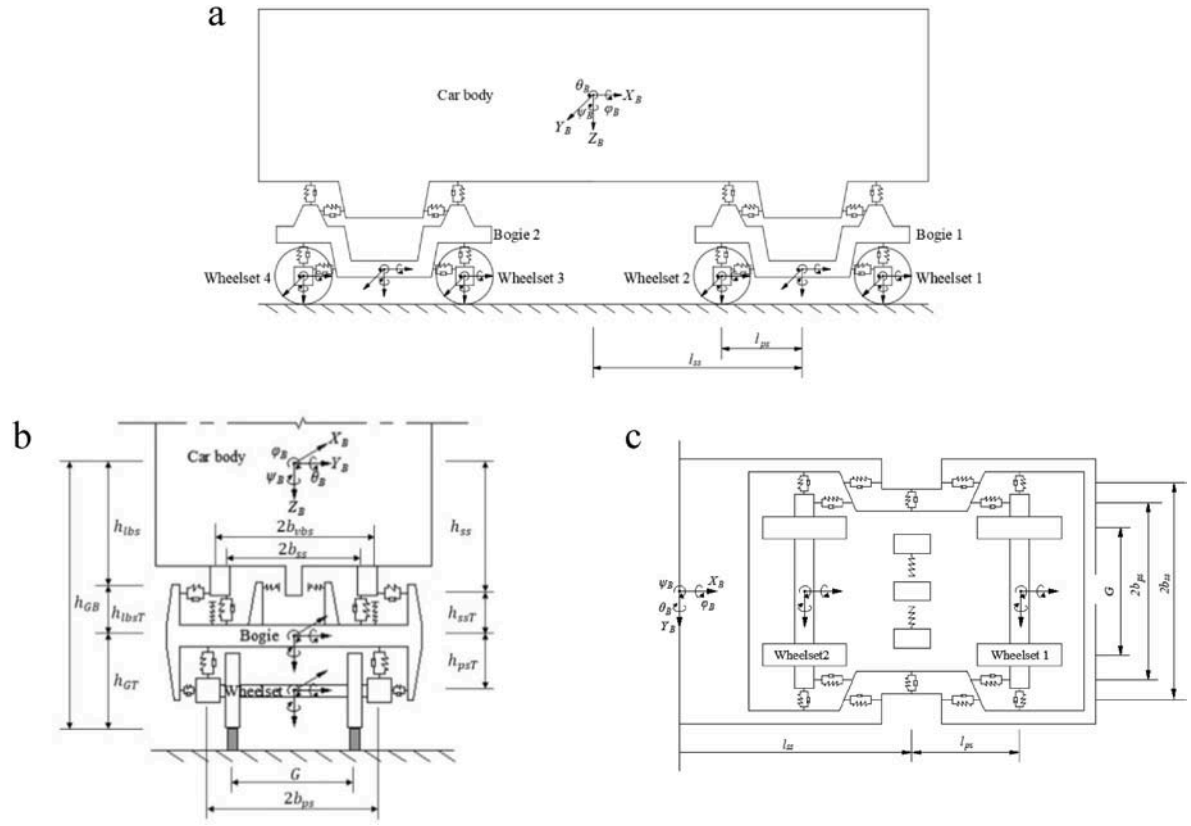

Fig. 4. A 42DoFs railway vehicle model: (a) side view; (b) end view; (c) top view.

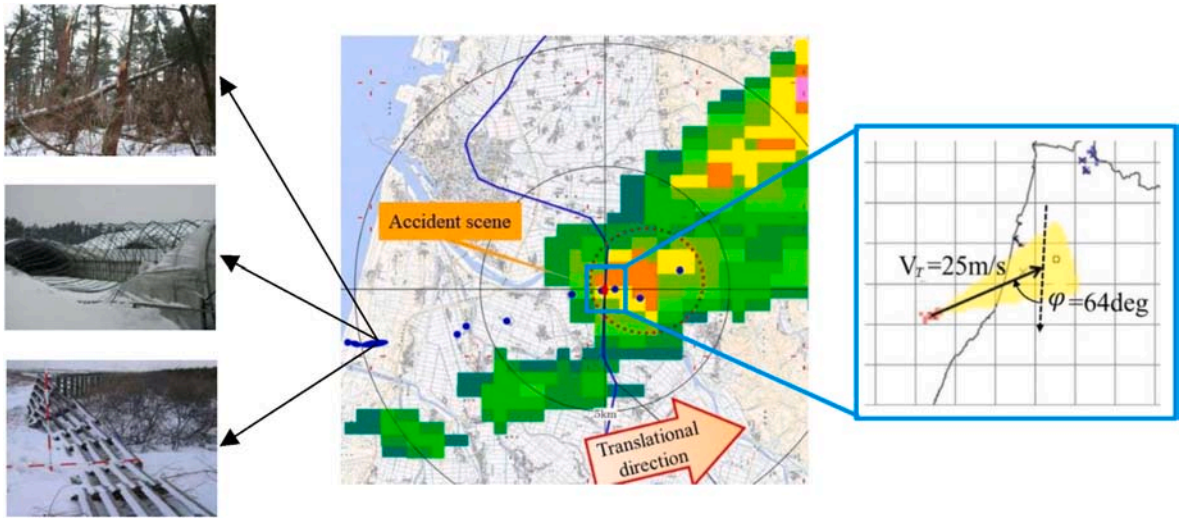

Fig. 5. The destruction along tornado path and radar echo intensity (ARAIC, 2008).

Table 1
Description of the tornado and the limited express train.

Items		Value	Reference
Tornado	Core radius	$R_{Max} = 30m$	NRA (2013)
	Translation velocity	$V_T = 25$m/s	ARAIC (2008)
	Direction of tornado path	$\varphi = 64deg.$	ARAIC (2008)
Train	Train speed	$V_{tr} = 100km/h$	ARAIC (2008)
	Train parameters	Provided	ARAIC (2008)
	Aerodynamic coefficients	Provided	ARAIC (2008)

of agricultural implements house near the track (Tamura et al., 2007). The tornado translated from the direction of 64° and intersected the track at 180m position as shown in Fig. 6. It was noticed that No. V power pole tilted, while No. VI and No. VII power poles broke. It implied that the limited express train capsized and then crashed the No. VI and No. VII power poles. The lateral distances from the track center to the No. VI and No. VII power poles were $d_{p6} = 3.75$ m and $d_{p7} = 3.65$ m, respectively as shown in Fig. 7(a). The lateral distance of the No. V power pole is unknown and is assumed as $d_{p5} = 3.65$ m as well. The power poles will be destroyed by the limited express train when the lateral displacements of the top left corner of car body are equal to or larger than 3.65m as shown in Fig. 7(b). Otherwise, they will not be demolished. It was found that the track was damaged between No. V and No. VI power poles which meant that the overturning presumably happened during this section.

The lateral displacement of the gravity center of car body is used to evaluate the railway vehicle overturning and the limited express train will turn over if the gravity center of car body moves outside the track (Chen and Chen, 2010). The distance between two rail/wheel contact

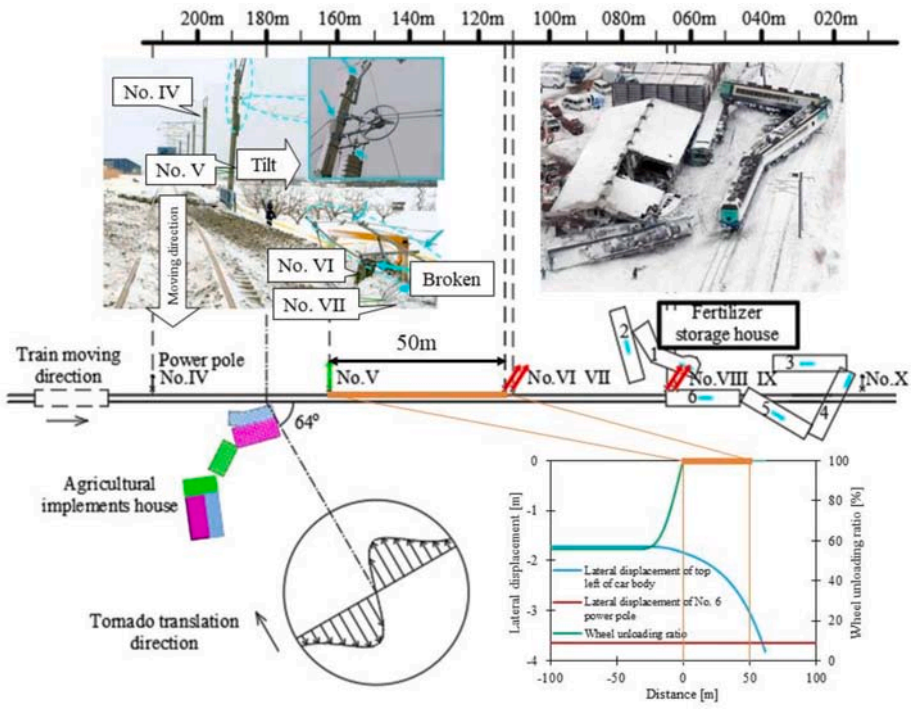

Fig. 6. The Uetsu line railway accident scene (ARAIC, 2008).

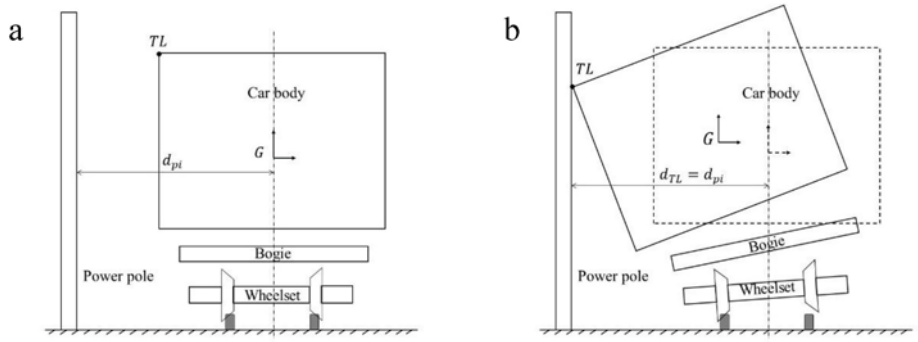

Fig. 7. Description of (a) lateral distance of the *No.i* power pole d_{pi} and (b) lateral displacement of the top left corner of car body.d_{TL}

points are 1.12m and it implies that the overturning occurs when the lateral displacement of the gravity center of car body is equal to or larger than 0.56m. Furthermore, the lateral displacement of the top left corner of car body d_{TL} from the track center is used to decide whether the power pole will be attacked by the limited express train as shown Fig. 7.

3. Results and discussions

The tangential velocities predicted by tornado models are compared with the measurement data, and tornado-induced aerodynamic forces calculated by the quasi-steady theory are validated by the experimental data in section 3.1. The Uetsu line railway accident is then studied by multibody dynamic simulations in section 3.2. Finally, the dynamic amplification factor (DAF) for railway vehicles in tornado winds is investigated and a simple method to predict the DAF is also proposed in section 3.3.

3.1. Validation of tornado-induced aerodynamic force model

In order to evaluate the accuracy of tornado models, the tangential velocities predicted by Rankine and Burgers-Rott models are compared with the measurement data. Tornadoes are frequently observed in the Japan Sea coastal region during winter due to vortex disturbances (Kobayashi et al., 2007; Inoue et al., 2011, Kato et al., 2015, Kusunoki et al., 2016). The tornadoes in this area have smaller core radius (30m–60m) and faster translational velocity ($V_T \approx (0.4 - 06)V_{Max.T}$), since the tornados observed in Japan are weaker than those detected in USA. Various type of facilities, namely, automated weather station, Doppler weather radar and Linear Array of Wind and Pressure Sensors (LAWPS) were built to detect and measure tornadoes in this region as shown in Fig. 8(a). The LAWPS consists of 12 anemometers and 25 barometers installed along the shoreline to measure wind speed and pressure near the ground. The anemometers were placed at the height of 5m at an interval of 100m, while the barometers were located at the height of 0.5m with an interval of 50m as shown in Fig. 8(b) and (c). A tornadic vortex near 1S in Fig. 8(c) was detected and measured by using the high-resolution Doppler radar and the LAWPS system by Kato et al. (2015). The translational velocity of the tornadic vortex was estimated by the Doppler radar and it was 16.1 m/s. The two-dimensional structure of wind speed of the tornadic vortex measured by the anemometers at 1S was converted from time to space according to translational velocity, translational direction and the Generic Mapping Tools, and the maximum tangential velocities in the forward and rearward regions were 27 m/s and 19 m/s (translational velocity was subtracted), respectively. Based on the least square method, fittings of two tornado models to the observations were carried out where the core radii R_{Max} in the forward and rearward regions were 55m and 35m, and the maximum tangential velocities of the stationary tornado $V_{Max.S}$ in the forward and rearward regions were 18 m/s and 22 m/s, respectively. Compared with the above measurement data, it is found that the tangential velocity predicted by the Burgers-Rott model shows good agreement with the measurement data in Fig. 9(a).

In this study, a simple method (ANS, 1983) is adopted to predict the translational velocity V_T and it is directly added to the stationary

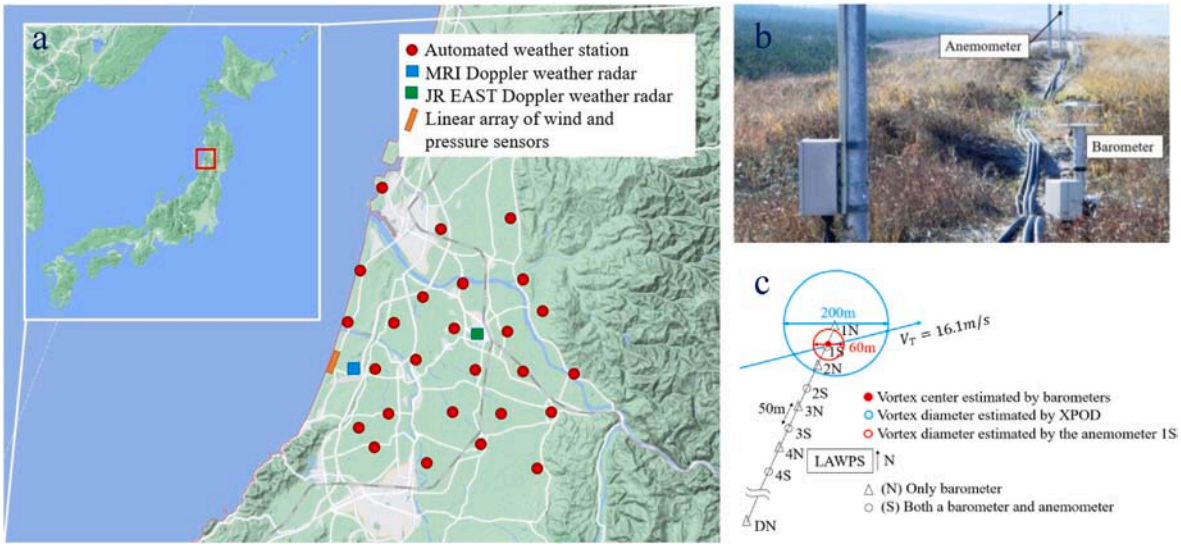

Fig. 8. The shonai area railroad weather project: (a) major facilities for the observation installed in Shonai area (Kusunoki et al., 2016); (b) photographs of the LAWPS (Kusunoki et al., 2016); (c) configuration of the tornado measured by Doppler weather radar and LAWPS (Kato et al., 2015).

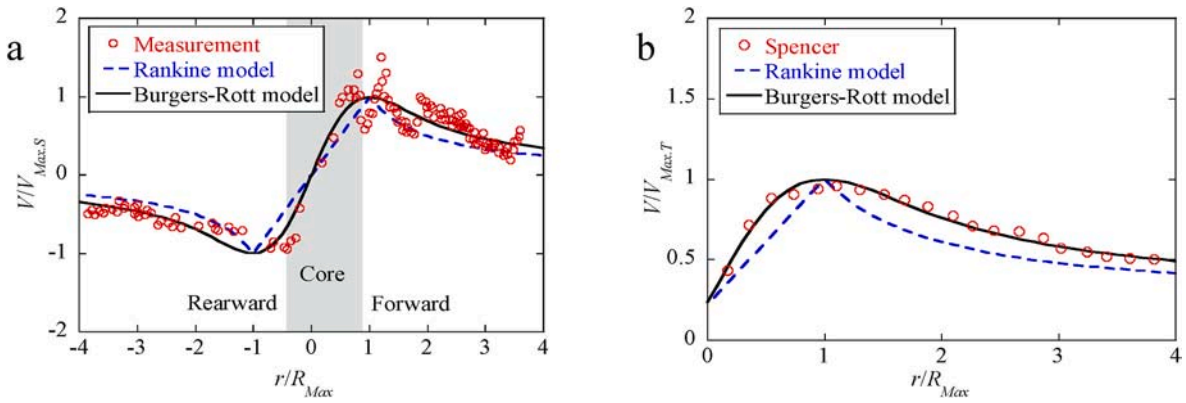

Fig. 9. Comparisons of tangential velocities between tornado models: (a) a stationary tornado (Kato et al., 2015); (b) and a moving tornado (Spencer).

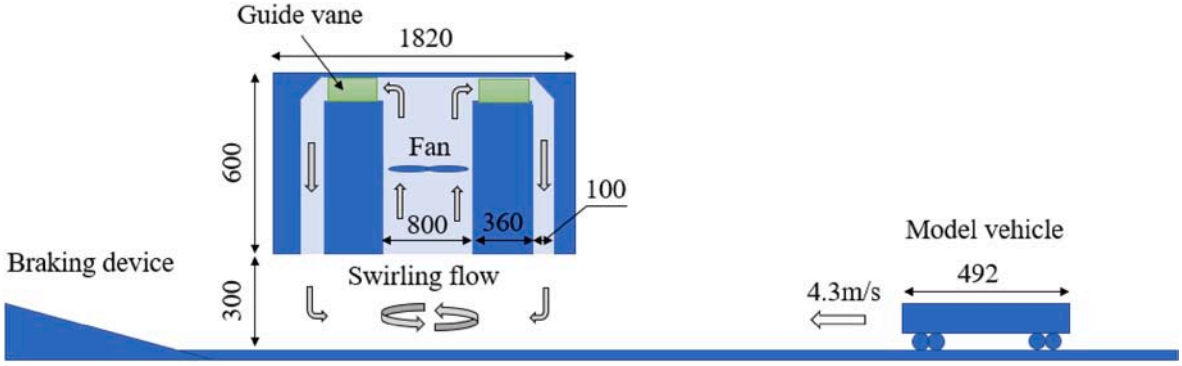

Fig. 10. Configuration of the experiment carried out by Suzuki and Okura (2016) (units: mm).

Table 2
Basic information of the experiment carried out by Suzuki and Okura (2016).

Items	Value
Core radius	100 mm
Maximum tangential velocity of a stationary tornado	8 m/s
Length of car body	492 mm
Train speed	4.3 m/s

tornado wind fields. The tangential velocity of a moving tornado predicted by the Burgers-Rott model matches well with the Spencer tornado (Kuai et al., 2008) as shown in Fig. 9(b), in which the translational velocity V_T is $0.22V_{Max.T}$ based on the guidance (ANS, 1983). Wurman and Alexander (2005) found that the translational velocity of the Spencer tornado changed between 10 m/s and 30 m/s, and the maximum tangential velocity was 81 m/s. Therefore, it is rational to assume that $V_T = 0.22V_{Max.T}$ in this case.

In summary, the Burgers-Rott model predicts the tangential velocity well in both stationary and moving tornadoes, while the Rankine model underestimates them.

The experiment was carried out by Suzuki and Okura (2016) to measure tornado-induced aerodynamic forces on the railway vehicle. As shown in Fig. 10, a 1/40 scale model vehicle passes through the tornado-like vortex generated by a stationary ISU-type tornado simulator. The core radius is 0.1m and the maximum tangential velocity is around 8 m/s at the height of 0.054 m. There are 72 pressure ports on the surfaces of car body, and pressure sensors are installed to measure the unsteady pressure induced by the swirling flow. Basic information of the experiment is summarized in Table 2.

The experimental data is used to validate the tornado-induced

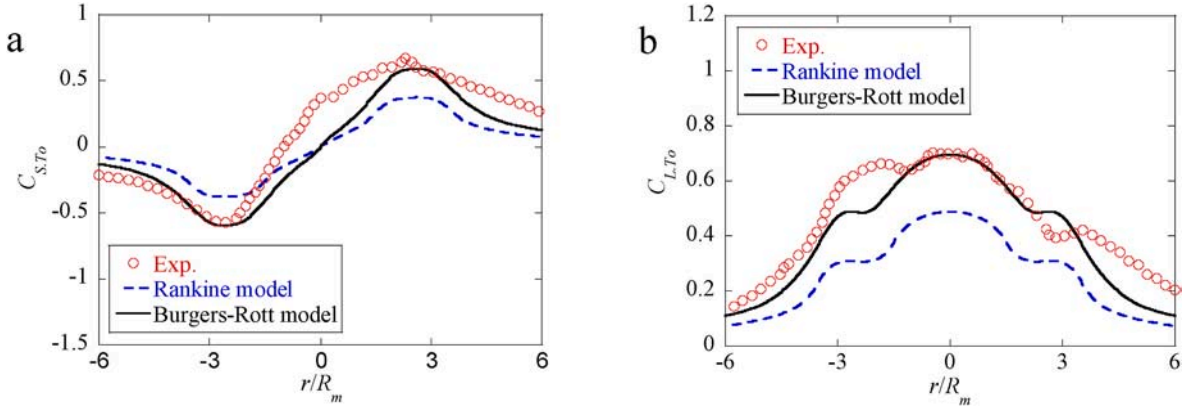

Fig. 11. Tornado-induced aerodynamic force coefficients: (a) side force coefficient; (b) lift force coefficient.

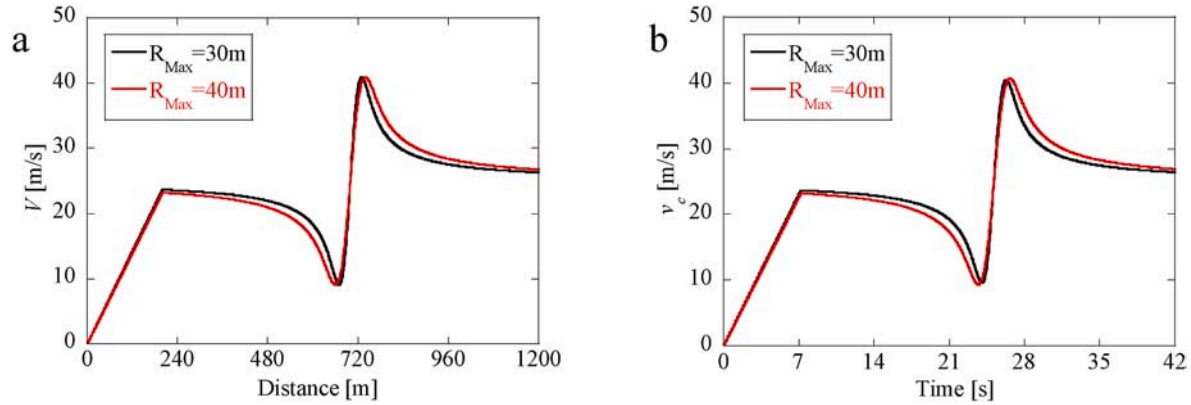

Fig. 12. The tangential velocity: (a) distributed along the track in spatial domain; (b) at the vehicle center in time domain ($V_{Max.T} = 41m/s$, $V_{tr} = 100km/h$).

aerodynamic force model as described in section 2.1. The aerodynamic coefficients of the commuter rail on the ground measured by Nagumo and Ishihara (2019) are used, although the geometries of the vehicle models are slightly different. As shown in Fig. 11, the tornado-induced side and lift force coefficients match well with the experimental data when the Burgers-Rott model is used. The discrepancies may be caused by the interaction between the running vehicle model and the tornado-like vortex since the tornado wind fields may be affected by the vehicle model when it passes through the tornado-like vortex.

3.2. Uetsu line railway accident reanalysis by multibody dynamic simulations

The Burgers-Rott model is adopted to predict the wind field of the tornado as mentioned in section 3.1. There are two approaches to deal with turbulent flows. One is the probabilistic approach using stochastic wind models, in which the turbulent flow is generated and used for the train stability analysis. The other is the deterministic approach, in which the 3s gust is used for the train stability analysis. The maximum responses of railway vehicle predicted by the deterministic approach showed good agreement with those obtained from the measurements of the prototype railway vehicle as shown in Ishihara et al. (2021). In this study, tornado-wind speed is simulated in a similar way as the Chinese hat gust model without turbulence (EN 14067-6, 2010).

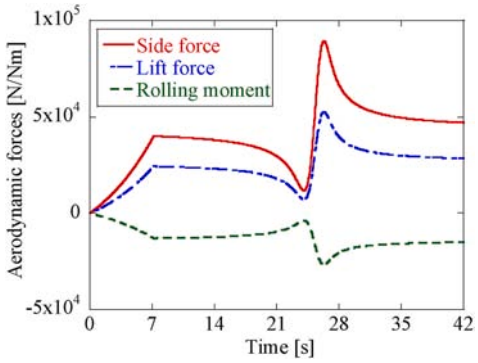

Fig. 13. Tornado-induced aerodynamic forces ($V_{Max.T} = 41m/s$, $R_{Max} = 30m$, $V_{tr} = 100km/h$).

The tangential velocity of the tornado is assumed to be distributed along the track as shown in Fig. 12(a). The wind speed increases from zero to the tangential velocity of the translational tornado and the tornado center is located at the distance of 700 m. The temporal wind speed at the railway vehicle center is calculated by using the equivalent wind force method as shown in Fig. 12(b), where the length of one carriage is around 20 m and the train speed is 100 km/h. Finally, the tornado-induced aerodynamic forces and moment on railway vehicle are calculated by the quasi-steady theory as shown in Fig. 13.

Fig. 14 shows the predicted dynamic responses of the limited express train in tornado winds. The first carriage is considered in the simulation since it was suddenly hit by the strong winds as stated by the driver. It is noted that the maximum lateral displacement of gravity center of car body is around 0.22 m when the maximum tangential velocity $V_{Max.T}$ is 36 m/s as shown in Fig. 14(a), therefore, the limited express train will not turn over. At this case, the maximum wheel unloading ratio has reached 100% and maintains this value for several seconds as shown in Fig. 14(b), which means that the limited express train is running forward with wheels on the windward side lifting. It is consistent with the conclusion by Hibino et al. (2013b) that the railway vehicle will not turn over even if wheel unloading ratio increases to 100%. The lateral displacement and wheel unloading ratio then reduce as aerodynamic forces decrease, which means the railway vehicle returns to the track.

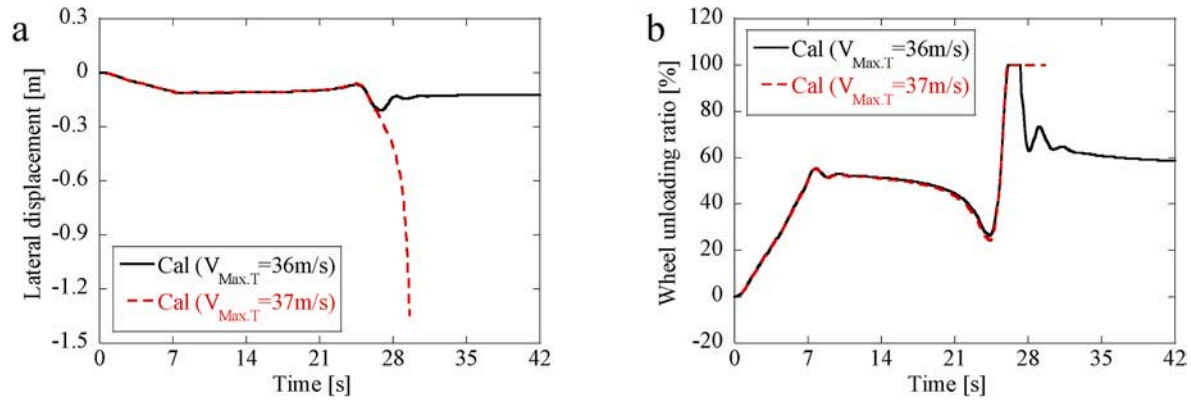

Fig. 14. Predicted dynamic responses of the limited express train in tornado winds ($R_{Max} = 30m$): (a) lateral displacement of the gravity center of car body and (b) wheel unloading ratio.

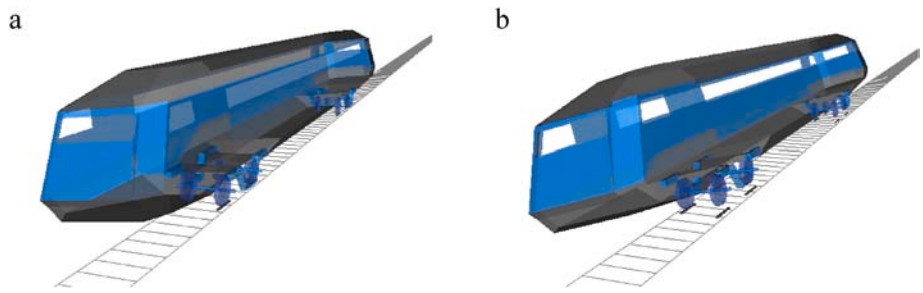

Fig. 15. Configuration of (a) lifting and (b) overturning of car body by the numerical simulations (calculated by SIMPACK (Dassault Systems, 2017)).

Table 3
Variations of dynamic responses with the maximum tangential velocities and core radii.

Radius	$V_{Max.T}$ [m/s]	35	36	37	38	39	40	41	42	43
R_{Max} = 30m	Lifting	No	Yes	Yes	Yes	Yes	Yes	Yes	Yes	Yes
	Overturning	No	No	Yes	Yes	Yes	Yes	Yes	Yes	Yes
	Distance between lifting and crashing positions [m]	–	–	100	67	59	53	50	47	44
R_{Max} = 40m	Lifting	No	Yes	Yes	Yes	Yes	Yes	Yes	Yes	Yes
	Overturning	No	No	No	Yes	Yes	Yes	Yes	Yes	Yes
	Distance between lifting and crashing positions [m]	–	–	–	85	68	60	54	51	48

Table 4
Variations of lifting, overturning and crashing positions with maximum tangential velocities and core radii.

$V_{Max.T}$	R_{Max} = 30m			R_{Max} = 40m		
	Lifting position	Overturning position	Crashing position	Lifting position	Overturning position	Crashing position
37	158m	85m	58m	–	–	–
38	160m	116m	93m	153m	88m	69m
39	161m	124m	103m	156m	105m	88m
40	162m	125m	109m	158m	114m	98m
41	163m	133m	113m	160m	121m	106m
42	164m	135m	117m	161m	125m	110m
43	164m	138m	120m	162m	128m	114m

However, the limited express train will turn over when the maximum tangential velocity $V_{Max.T}$ increases to 37 m/s since the maximum lateral displacement of gravity of car body is larger than 0.56 m. Fig. 15 shows configurations of lifting (wheel unloading ratio equal to 100%) and overturning (lateral displacement of the gravity center of car body equal to 0.56 m) by the numerical simulations. Note that the same parameters of railway vehicle are used in multi-body simulations for the accident investigation, including the rolling out of the line since the geometric nonlinearity is dominant in the final stage of simulation.

The predicted dynamic responses of the limited express train for each maximum tangential velocities and core radius are summarized in Table 3. It is found that wheel unloading ratio starts to become 100% when the maximum tangential velocity increases to 36 m/s, however, the vehicle will not turn over until it rises to 37 m/s. Table 4 shows the lifting (the wheel unloading ratio is 100%), the overturning (when the lateral distance of the gravity center of car body is 0.56 m) and the distance between lifting and crashing positions (the No. VI power pole is crashed). This distance is most close to the distance between No. V and No. VI power poles when the maximum tangential velocity is 41 m/s, In this case, the railway accident scene is well reproduced, that is, the No. V power pole will not be touched, while the car body will hit the No. VI power pole, and the overturning happens between them as shown in Fig. 6.

As mentioned above, the core radius of tornado is unknown in the accident investigation report and it is assumed to be 30 m in this study. To investigate the effect of core radius of tornado in the dynamic response, a case with the core radius of 40 m is added. As the core radius increases from 30 m to 40 m, the vehicle will lift and turn over when the

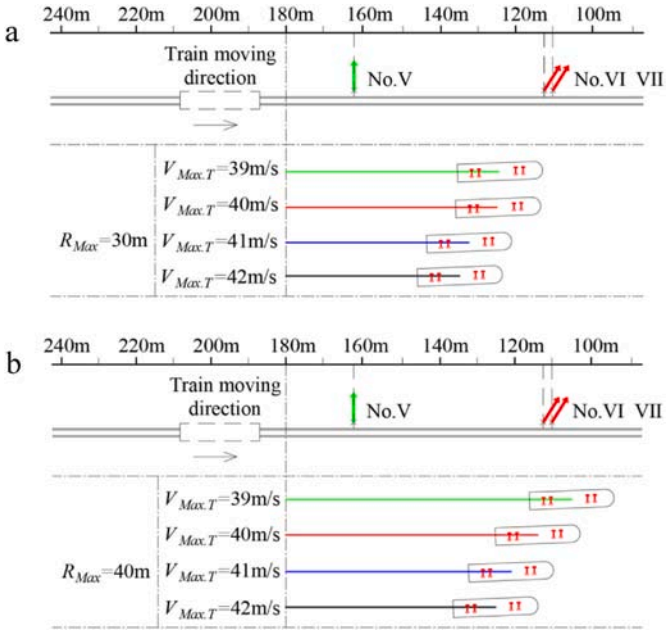

Fig. 16. Variations of overturning positions of the first carriage with core radius of (a) 30m and (b) 40m.

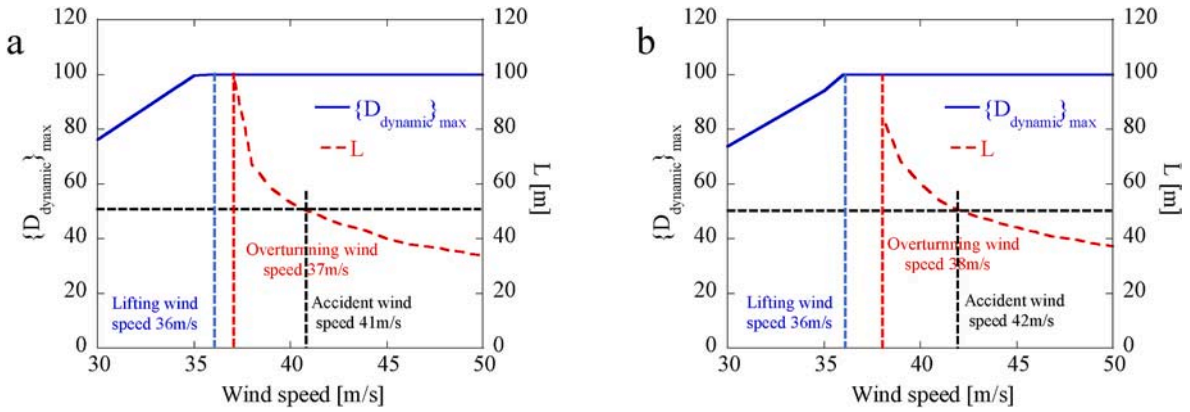

Fig. 17. Variations of maximum wheel unloading ratio and the distance between lifting and crashing positions with maximum tangential wind speed: (a) $R_{max} = 30m$ (b).$R_{max} = 40m$

maximum tangential velocity increases to 37 m/s and 38 m/s, respectively, as shown in Table 3. The lifting, overturning and crashing positions change slightly and the influence of core radius on the dynamic responses is negligible as shown in Table 4 and in Fig. 16.

Furthermore, the variations of maximum wheel unloading ratio and the distance between lifting and crashing positions (L) are illustrated in Fig. 17. It is distinct that the wheel unloading ratio reaches 100% when the maximum tangential velocity is 36 m/s for both cases. Afterwards, the railway vehicle turns over as the maximum tangential velocities increase to 37 m/s and 38 m/s for the two cases where $R_{Max} = 30m$ and $R_{Max} = 40m$, respectively. It is found that the distance between lifting and crashing positions is around 50m when the maximum tangential velocities increase to 41 m/s and 42 m/s for the two cases, which is coincident with accident scene as shown in Fig. 6. Therefore, it is believed that the limited express train turns over at the maximum tangential velocity around 41–42 m/s.

In summary, the predicted accident scenes show favorably agreement with those obtained from the accident survey, in which the No. V power pole will not be pulled down, but the No. VI power pole is totally destroyed, and the distance before crashing No. VI power pole is equal to the distance between No. V and No. VI power poles when the maximum tangential velocity is around 41 m/s.

3.3. Dynamic amplification factor in tornado winds

The dynamic amplification factor (DAF) defined in Eq. (10) by Ishihara et al. (2021) is used to account for the railway vehicle dynamics including the effects of damping and inertial forces in the multi-body simulations, which are ignored in the quasi-static analysis.

$$DAF = \frac{max\{D_{dynamic}\}}{D_{static}} \tag{10}$$

where D_{static} and $D_{dynamic}$ represent the static and dynamic wheel unloading ratios calculated by quasi-static analysis and multibody dynamic simulations, respectively. The DAF is expressed in terms of vehicle dynamics. The increase of lateral displacement and roll angle of vehicle reduces forces transmitted to ground as shown in Ishihara et al. (2021).

The DAF for railway vehicles in tornado winds is also studied. The core radius R_{Max} changes from 20 m to 40 m. The maximum wind speeds are selected as 20 m/s and 25 m/s considering the lower and higher limit of the F0 scale tornado are 17 m/s and 32 m/s. On the one hand, it is not necessary to study the case with the wind speed smaller than 17 m/s. On the other hand, the wheel unloading ratio will be larger than 100% when the maximum tangential velocity is larger than 29 m/s for the commuter rail (E233 series) as shown in Ishihara et al. (2021). The E233 is widely used in JR-EAST and lighter than the railway vehicle used in the Uetsu line. Furthermore, in accidence with the guideline (NRA, 2013), the translational velocity of tornado is defined as $V_T = c_t V_{Max.T}$, where c_t is equal to 0.15. The effects of c_t is included in Eq. (11) and discussed in Fig. 23. Six cases are investigated, in which the core radius R_{Max} and the maximum tangential velocity $V_{Max.T}$ vary as shown in Table 5. The train speed is another dominant parameter and affects the DAF. Therefore, the train speed V_{tr} is systematically changed from 20 km/h to 120 km/h at 20 km/h increments. The wind distribution in space domain and the temporal wind speed at the railway vehicle center are the same as those as shown in Fig. 12.

Table 5
Simulation cases and the tornado wind parameters.

Case	R_{Max} [m]	$V_{Max.T}$ [m/s]	V_{tr} [km/h]
1	20	20	20–120 at 20 increments
2	20	25	20–120 at 20 increments
3	30	20	20–120 at 20 increments
4	30	25	20–120 at 20 increments
5	40	20	20–120 at 20 increments
6	40	25	20–120 at 20 increments

The multibody dynamic model of the commuter rail (E233 series) is used in this study to investigate the DAF in tornado winds, which was validated and the corresponding DAF under tunnel exit winds was investigated by Ishihara et al. (2021). The static and dynamic wheel unloading ratios are calculated by the quasi-static analysis and multibody dynamic simulations, respectively, as shown in Fig. 18. The maximum wheel unloading ratios calculated by the multibody dynamic simulations are larger than those obtained by the quasi-static analysis. As illustrated in Fig. 18(a), both dynamic and static wheel unloading ratios maintain the same value as the core radius increases since the temporal wind speeds at vehicle center change slightly. However, the difference between multibody dynamic simulations and the quasi-static analysis becomes more obvious as the maximum tangential velocity of tornado or the train speed increases as shown in Fig. 18(b) and (c). It is found that the maximum wheel unloading ratios calculated by two methods are completely the same when the train speed is around 20 km/h. It implies that the DAF is negligible when the train speed is low and the wheel unloading ratios can be accurately predicted by the quasi-static analysis.

An exponential formula was proposed by Ishihara et al. (2021) to evaluate the DAF for railway vehicles in tunnel exit winds, in which the DAF increases as the passing time decreases. In this study, the exponential formula is expressed as Eq. (11).

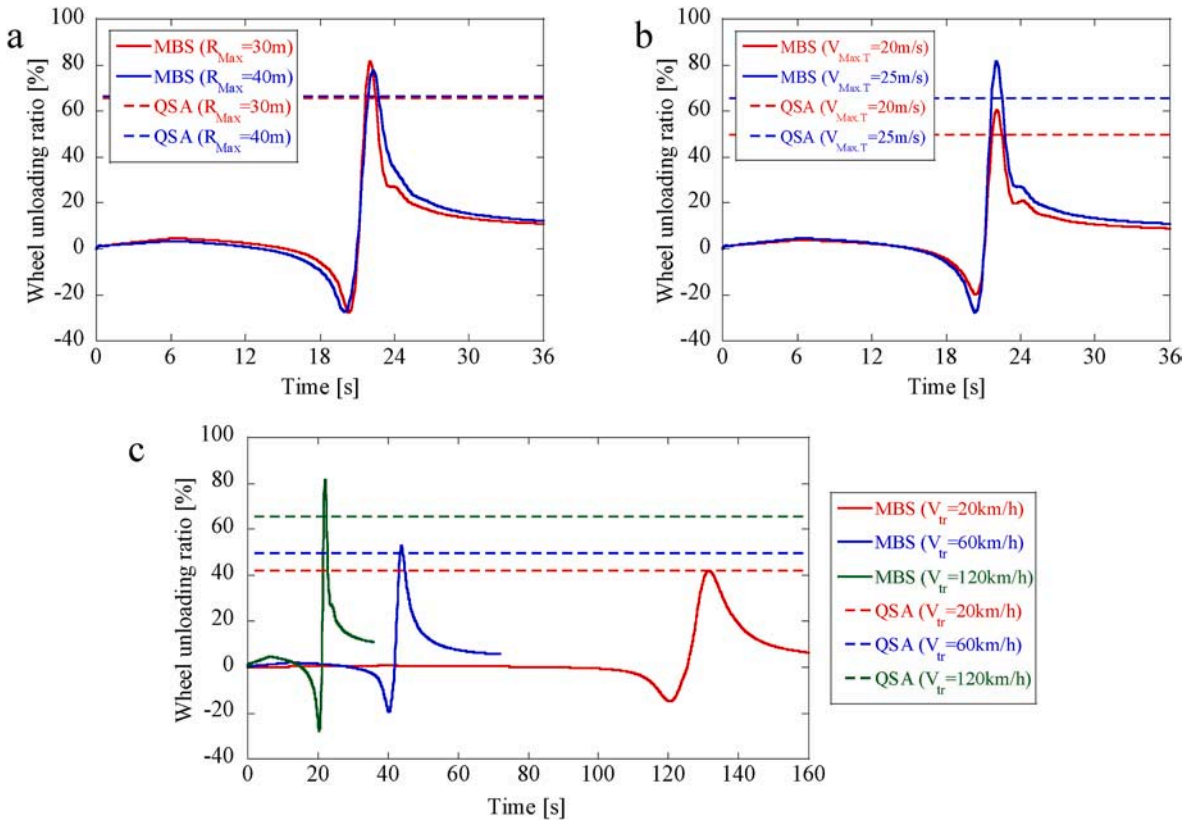

Fig. 18. Variations of wheel unloading ratio with: (a) core radius ($V_{Max.T} = 25m/s$, $V_{tr} = 120km/h$); (b) maximum tangential wind speed ($R_{Max} = 30m$, $V_{tr} = 120km/h$); (c) train velocity ($R_{Max} = 30m$, $V_{Max.T} = 25m/s$)

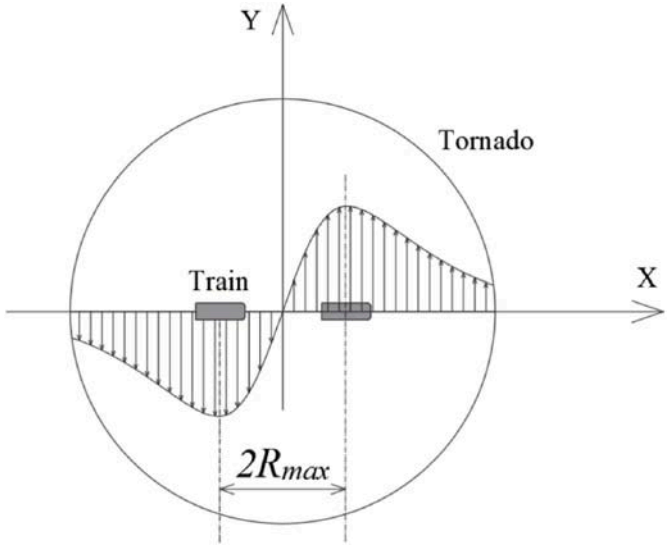

Fig. 19. The passing time Δt in tornado winds.

$$\begin{aligned} DAF &= c \cdot e^{\left[-a(\Delta t)^b\right]} + 1, \\ \Delta t &= (L_1 + L_2) \Big/ V_{tr}, \\ \mathrm{c} &= (1 - c_t) \Big/ (1 - 0.15) \end{aligned} \tag{11}$$

where a and b are parameters which are related to the natural frequency f_n of the first rolling mode of the car body and the damping ratio ζ. c is a function of ratio of translational velocity to maximum tangential velocity c_t. It decreases to 0 when $c_t = 1$, which means that the tornado wind disappears, and approaches to 1 when $c_t = 0.15$ since parameters a and b are identified for the case of $c_t = 0.15$. Δt is the time that the railway vehicle totally passes through the core radius as shown in Fig. 19, L_1 and L_2 are the maximum radius in the forward and rearward regions of tornado and equal to R_{Max}.

The maximum value of dynamic wheel unloading ratio $D_{dynamic}$ can be calculated by Eq. (12).

$$D_{dynamic} = DAF \cdot D_{static} \tag{12}$$

where D_{static} is the static wheel unloading ratio calculated by the quasi-static analysis.

The DAF for the commuter rail in tornado winds is then calculated by the ratio of dynamic and static wheel unloading ratios as shown in Eq. (10). It is found that the DAF increases as the passing time decreases in Fig. 20. The DAF in tornado winds shows the same trend with that in tunnel exit winds. However, the maximum value for the commuter rail (E233 series) in tornado winds is around 1.32, and it is a little larger than that (around 1.25) in the tunnel exit wind. Similar to the tunnel exit wind, the dynamic amplification effect is obvious when the wind speed sharply increases, otherwise, it is negligible.

Effect of natural frequency and damping ratio on the DAF for railway vehicle under tunnel exit winds are quantitatively studied by Ishihara et al. (2021). Five different natural frequencies are considered by changing either the mass of car body or the stiffness in the second suspension system as shown in Table 6. They will vary 3/4 and 5/4 times as large as the prototype value and the horizontal (K_{ys}) and vertical (K_{zs}) stiffness will change simultaneously. The eigenvalue analysis is used to predict the natural frequency of each case.

The equivalent damping ratio of railway vehicles defined by Ishihara et al. (2021) is used and written as:

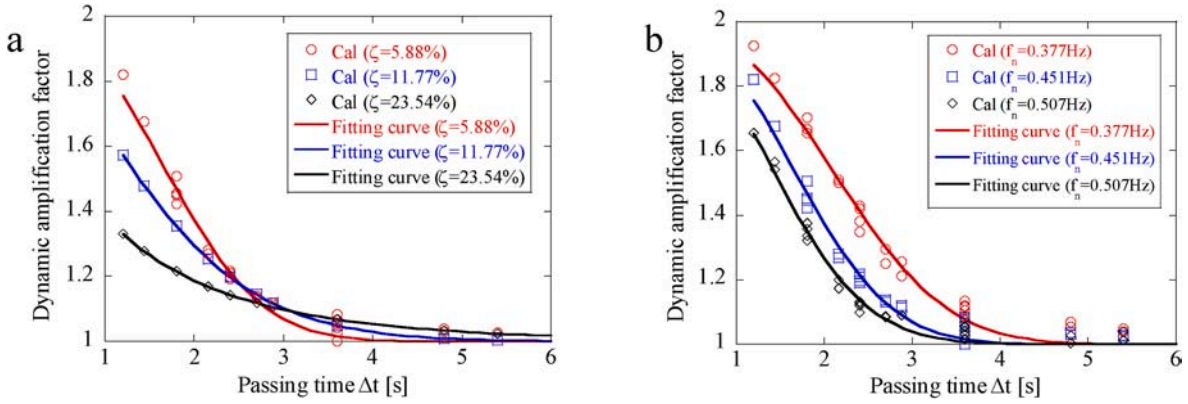

Fig. 20. Variations of DAF with the passing time as functions of (a) damping ratio ($f_n = 0.451Hz$) and (b) natural frequency ($\zeta = 5.88\%$).

Table 6
Five cases to describe natural frequencies.

Case	$m_B/\{m_B\}_{original}$	$K_{ys}/\{K_{ys}\}_{original}$	$K_{zs}/\{K_{zs}\}_{original}$	f_n [Hz]
1	1	1	1	0.451
2	3/4	1	1	0.508
3	5/4	1	1	0.400
4	1	3/4	3/4	0.377
5	1	5/4	5/4	0.507

Table 7
Three cases to describe damping ratios.

Case	ζ_l	ζ_v	ζ
1	25.80%	21.28%	23.54%
2	12.9%	10.64%	11.77%
3	6.45%	5.32%	5.88%

$$\zeta = \frac{\zeta_l + \zeta_v}{2} \quad \left(\zeta_v = \frac{D_{zs}}{2\sqrt{4K_{zs}m_B}}, \zeta_l = \frac{D_{ys}}{2\sqrt{4K_{ys}m_B}}\right) \tag{13}$$

where D_{zs} and D_{ys} are vertical and horizontal damping parameters in the second suspension system, respectively. K_{zs} and K_{ys} are stiffness in horizontal and vertical directions in second suspension, and m_B refers to the mass of car body. ζ_v, ζ_l and ζ are defined as vertical, horizontal and total equivalent damping ratios. Table 7 shows three different equivalent damping ratios and they decrease 1/2 and 1/4 times as large as the prototype value.

The DAF for railway vehicle in tornado winds are calculated by taking account of five different natural frequencies and three damping ratios and several cases are illustrated in Fig. 20. It is found that the DAF can be effectively suppressed as the damping parameters increase in Fig. 20(a) while it decreases slightly as the natural frequency increases in Fig. 20(b), similar to those in tunnel exit winds.

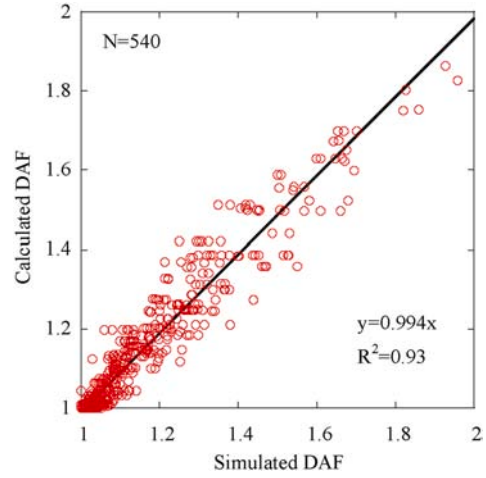

Fig. 22. Comparisons of the simulated and predicted DAF by Eq. (11).

Subsequently, a and b in Eq. (11) for each case are calculated by fitting curve of the DAF. It is assumed that a and b in Eq. (11) change linearly with the natural frequency and the equivalent damping ratio when the natural frequency changes from 0.377Hz to 0.508Hz and the

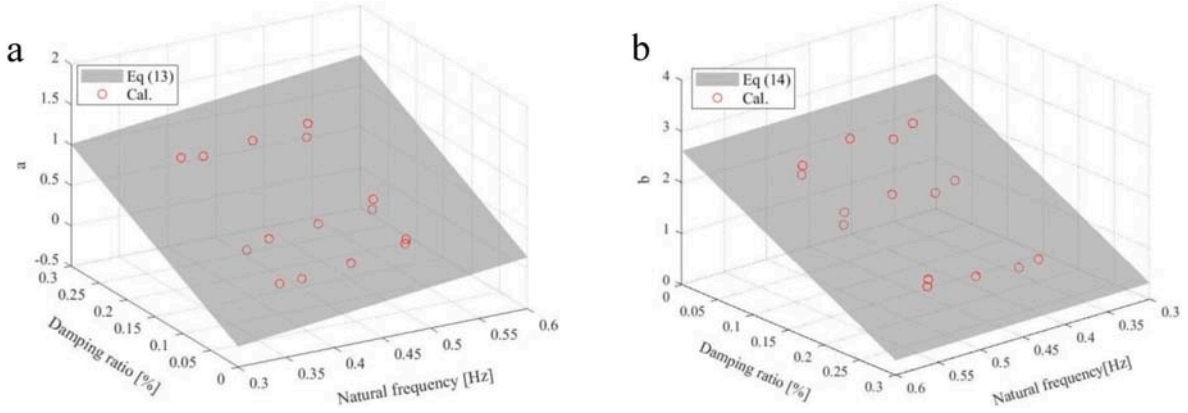

Fig. 21. Fitting surfaces of (a) $a(f_n, \zeta)$ and (b) $b(f_n, \zeta)$ with natural frequency and equivalent damping ratio.

Table 8
Description of parameters used in the simulations.

Case	R_{Max} [m]	V_{tr} [km/h]	$V_{Max.T}$ [m/s]	c_t –
1	20–40	120	25	0.15
2	20	20–120	25	0.15
3	20	120	20–25	0.15
4	20	120	25	0.1–0.7

damping ratio changes from 5.88% to 23.54%. The least square method is adopted to obtain the fitting surface of a and b shown as Eqs. (14) and (15) and drawn in Fig. 21.

$$a(f_n, \zeta) = -0.628 + 1.278 f_n + 4.172\zeta \tag{14}$$

$$b(f_n, \zeta) = 2.676 - 0.102 f_n - 7.769\zeta \tag{15}$$

In order to evaluate the accuracy of the proposed method presented in Eq. (11) (14) and (15), the simulated and predicted DAF are compared and the coefficient of determination is also calculated $R^2 = 0.93$ in Fig. 22.

A sensitivity study on the DAF and the dynamic wheel unloading ratio is performed considering the effects of core radius, train speed, maximum tangential velocity and ratio of translational velocity to maximum tangential velocity. Table 8 describes the parameters used in the simulations. Fig. 23 shows the DAF and the dynamic wheel unloading ratio by the multi-body simulation (MBS) and those calculated by Eqs. (11) and (12). The static wheel unloading ratio by the quasi-static analysis (QSA) is also illustrated in Fig. 23 for comparison.

It is noticed that the DAF decreases as the core radius R_{Max} increases because the passing time increases (Fig. 23(a)). The dynamic wheel unloading ratio decreases due to the decrease of the DAF. On the other hand, the DAF increases as the train speed V_{tr} increases (Fig. 23(b)). As a result, the dynamic wheel unloading ratio significantly increases comparing with the static one. It implies that the regulation of train speed is useful when a strong tornado wind is detected. The maximum tangential velocity $V_{Max.T}$ has no effect on the DAF as illustrated in Fig. 23(c), while the dynamic wheel unloading ratio increases as the static wheel unloading ratio increases. Furthermore, the DAF decreases as the ratio of translational velocity to maximum tangential velocity c_t increases, which results in the decrease of dynamic wheel unloading ratio as shown in Fig. 23(d).

In summary, the dynamic wheel unloading ratios are larger than the static ones and the DAF should be considered in the tornado winds. The dynamic wheel unloading ratio can be predicted by Eq. (12) as the product of the static wheel unloading ratio obtained from the quasi-static analysis and the DAF calculated by Eq. (11).

4. Conclusions

In this study, the tornado-induced unsteady crosswind response of railway vehicles and the Uetsu line railway accident are investigated using multibody dynamic simulations. A dynamic amplification factor for railway vehicles in tornado winds is proposed. The conclusions are summarized as follows:

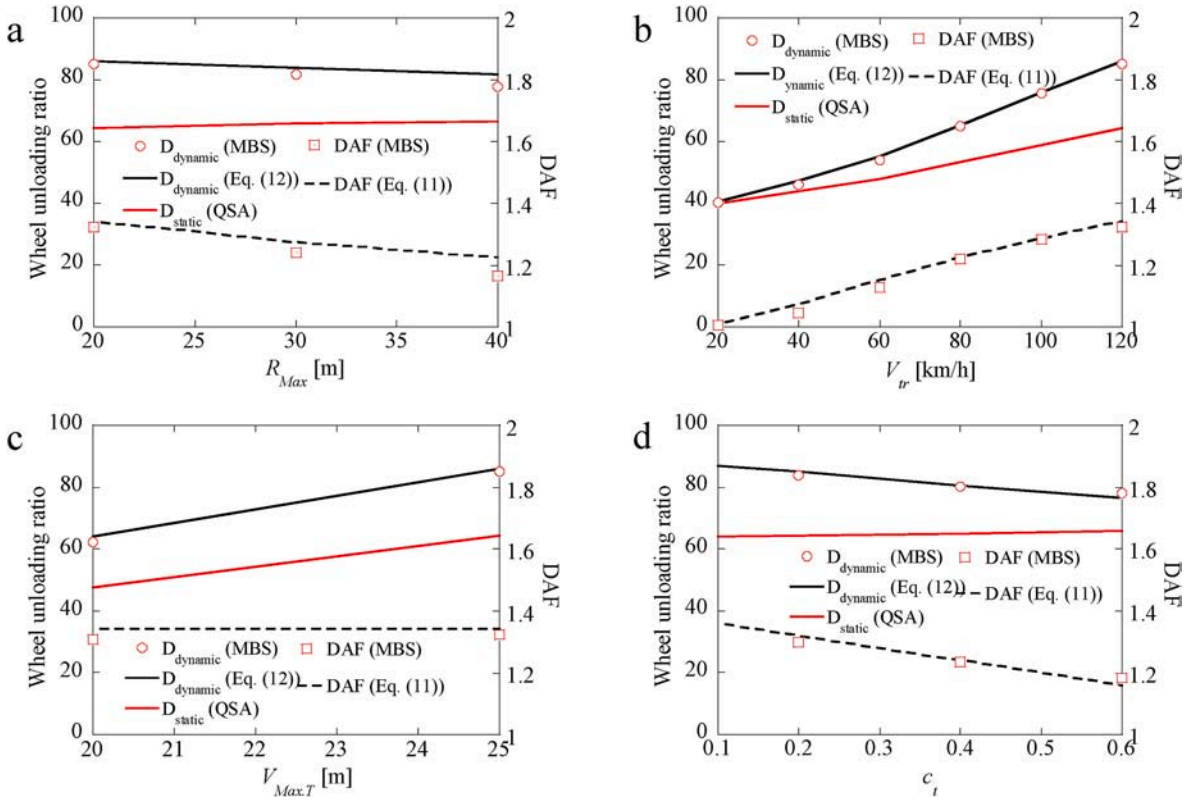

Fig. 23. Variation of wheel unloading ratio and the DAF with: (a) core radius R_{Max}; (b) train speed V_{tr}; (c) maximum tangential velocity $V_{Max.T}$; (d) ratio of translational velocity to maximum tangential velocity.c_t

(1) The tornado-induced aerodynamic forces on railway vehicle are accurately predicted by the quasi-steady theory after the temporal wind speed at the railway vehicle center is calculated by using the equivalent wind force method.
(2) The Uetsu line railway accident is reproduced using multi-body dynamic simulations. It is found that the simulation results are obviously affected by the maximum tangential velocity of tornado, but the effects of the core radius are negligible.
(3) The DAF for railway vehicles in tornado winds is investigated and a simple method to predict the DAF is proposed. It is observed that the DAF increases as the passing time decreases. The DAF can be effectively suppressed as the damping parameters increase while it decreases slightly as the natural frequency increases.

CRediT authorship contribution statement

Dongqin Zhang: Investigation, Software, Writing – original draft, Formal analysis, Visualization. **Takeshi Ishihara:** Resources, Conceptualization, Methodology, Supervision, Writing – review & editing.

Declaration of competing interest

The authors declare that they have no known competing financial interests or personal relationships that could have appeared to influence the work reported in this paper.

Acknowledgements

This study is carried out as a joint research program supported by East Japan Railway Company. The authors would like to acknowledge Dr. Yosuke Nagumo for providing the measurement data.

References

ANS, 1983. "Standard for Estimating Tornado and Extreme Wind Characteristics at Nuclear Power Sites" ANSI/ANS-2.3-1983.
ARAIC, 2008. The Railway Accident Investigation Report: RA2008-4. Japan.
Baker, C., Cheli, F., Orellano, A., Paradot, N., Proppe, C., Rocchi, D., 2009. Cross-wind effects on road and rail vehicles. Veh. Syst. Dyn. 47, 983–1022.
Baker, C.J., Sterling, M., 2018. The calculation of train stability in tornado winds. J. Wind Eng. Ind. Aerod. 176, 158–165.
Bourriez, F., Soper, D., Baker, C., Sterling, M., 2019. Physical Model Measurement of Tornado Induced Forces on Trains. Presented at the 15th International Conference on Wind Engineering, Beijing, pp. 429–430.
Burgers, J.M., 1948. A mathematical model illustrating the theory of turbulence. Adv. Appl. Mech. 1, 171–199.
Cao, J., Cao, S., Ge, Y., 2019. Experimental Investigations of Wind Load Distributions on a High-Speed Train under Tornado-like Vortices. Presented at the 15th International Conference on Wind Engineering, Beijing, pp. 437–438.
Cheli, F., Corradi, R., Rocchi, D., Tomasini, G., Maestrini, E., 2010. Wind tunnel tests on train scale models to investigate the effect of infrastructure scenario. J. Wind Eng. Ind. Aerod. 98, 353–362.
Cheli, F., Giappino, S., Rosa, L., Tomasini, G., Villani, M., 2013. Experimental study on the aerodynamic forces on railway vehicles in presence of turbulence. J. Wind Eng. Ind. Aerod. 123, 311–316.
Chen, S., Chen, F., 2010. Simulation-based assessment of vehicle safety behavior under hazardous driving conditions. J. Transport. Eng. 136, 304–315.
Dassault Systems, 2017. SIMPACK 2017.1 Simpack Assistant.
EN 14067-6, 2010. Railway applications - aerodynamics - Part6: requirements and test procedures for cross wind assessment. BS (Breed. Sci.) 14067-6, 2010.
Gillmeier, S., Sterling, M., Hemida, H., Baker, C.J., 2018. A reflection on analytical tornado-like vortex flow field models. J. Wind Eng. Ind. Aerod. 174, 10–27.
Heleno, R., Montenegro, P.A., Carvalho, H., Ribeiro, D., Calcada, R., Baker, C.J., 2021. Influence of the railway vehicle properties in the running safety against crosswinds. J. Wind Eng. Ind. Aerod. 217, 104732.
Hibino, Y., Kanemoto, H., Sakuma, Y., 2013a. A study on vehicle response to a sudden gust of wind. Trans. Jpn. Soc. Mech. Eng. Ser. C 79, 3410–3419 (in Japanese).
Hibino, Y., Kanemoto, H., Shimomura, T., 2013b. Safety evaluation of railway vehicle against crosswind applying a full-vehicle model. Q. Rep. RTRI 54, 133–138.
Hibino, Y., Shimomura, T., Tanifuji, K., 2010. Full-scale experiment on the behavior of a railway vehicle being subjected to lateral force. J. Mech. Syst. Transp. Logist. 3, 35–43.
Inoue, H.Y., Kusunoki, K., Kato, W., Suzuki, H., Imai, T., Takemi, T., Bessho, K., Nakazato, M., Hoshino, S., Mashiko, W., Hayashi, S., Fukuhara, T., Shibata, T., Yamauchi, H., Suzuki, O., 2011. Finescale Doppler radar observation of a tornado and low-level misocyclones within a winter storm in the Japan Sea coastal region. Mon. Weather Rev. 139, 351–369.
Ishihara, T., Zhang, D., Nagumo, Y., 2021. Numerical study of dynamic response of railway vehicles under tunnel exit winds using multibody dynamic simulations. J. Wind Eng. Ind. Aerod. 211, 104556.
Kato, R., Kusunoki, K., Sato, E., Mashiko, W., Inoue, H.Y., Fujiwara, C., Arai, K., Nishihashi, M., Saito, S., Hayashi, S., Suzuki, H., 2015. Analysis of the horizontal two-dimensional near-surface structure of a winter tornadic vortex using high-resolution in situ wind and pressure measurements. J. Geophys. Res. Atmos. 120, 5879–5894.
Kikuchi, K., Suzuki, M., 2015. Study of aerodynamic coefficients used to estimate critical wind speed for vehicle overturning. J. Wind Eng. Ind. Aerod. 147, 1–17.
Kim, Y.C., Matsui, M., 2017. Analytical and empirical models of tornado vortices: a comparative study. J. Wind Eng. Ind. Aerod. 171, 230–247.
Kobayashi, F., Sugimoto, Y., Suzuki, T., Maesaka, T., Moteki, Q., 2007. Doppler radar observation of a tornado generated over the Japan Sea coast during a cold air outbreak. J. Meteorol. Soc. Jpn. 85, 321–334.
Kuai, L., Haan Jr., F.L., Gallus Jr., W.A., Sarkar, P.P., 2008. CFD simulations of the flow field of a laboratory-simulated tornado for parameter sensitivity studies and comparison with field measurements. Wind Struct. 11, 75–96.
Kusunoki, K., Arai, K., Kato, R., Sato, E., 2016. A linear array of wind and pressure sensors for high resolution in situ measurements in winter tornadoes. IEEJ Trans. Fundam. Mater. 136, 286–290.
Liu, D., Lu, Z., Zhong, M., Cao, T., Chen, D., Xiong, Y., 2018. Measurements of car-body lateral vibration induced by high-speed trains negotiating complex terrain sections under strong wind conditions. Veh. Syst. Dyn. 56, 173–189.
Liu, D., Wang, Q., Zhong, M., Lu, Z., Wang, J., Wang, T., Lv, S., 2019. Effect of wind speed variation on the dynamics of a high-speed train. Veh. Syst. Dyn. 57, 247–268.
Liu, D., Wang, T., Liang, X., Meng, S., Zhong, M., Lu, Z., 2020. High-speed train overturning safety under varying wind speed conditions. J. Wind Eng. Ind. Aerod. 198, 104111.
Maleki, S., Burton, D., Thompson, M.C., 2017. Assessment of various turbulence models (ELES, SAS, URANS and RANS) for predicting the aerodynamics of freight train container wagons. J. Wind Eng. Ind. Aerod. 170, 68–80.
Montenegro, P.A., Barbosa, D., Carvalho, H., Calçada, R., 2020. Dynamic effects on a train-bridge system caused by stochastically generated turbulent wind fields. Eng. Struct. 211, 110430.
Montenegro, P.A., Carvalho, H., Ribeiro, D., Calçada, R., Tokunaga, M., Tanabe, M., Zhai, W.M., 2021. Assessment of train running safety on bridges: a literature review. Eng. Struct. 241, 112425.
Nagumo, Y., Ishihara, T., 2019. A study of aerodynamic coefficients on a train car considering turbulence effects of approaching flow. J. Wind Eng. 44, 90–104.
Neto, J., Montenegro, P.A., Vale, C., Calçada, R., 2021. Evaluation of the train running safety under crosswinds - a numerical study on the influence of the wind speed and orientation considering the normative Chinese Hat Model. Int. J. Rail Transp. 9, 204–231.
Niu, J., Zhou, D., Liu, T., Liang, X., 2017. Numerical simulation of aerodynamic performance of a couple multiple units high-speed train. Veh. Syst. Dyn. 55, 681–703.
Noguchi, Y., Suzuki, M., Baker, C., Nakade, K., 2019. Numerical and experimental study on the aerodynamic force coefficients of railway vehicles on an embankment in crosswind. J. Wind Eng. Ind. Aerod. 184, 90–105.
NRA, 2013. The Assessment Guidance for Tornado Effect on Nuclear Power Plants (in Japanese).
Olmos, J.M., Astiz, M.Á., 2018. Improvement of the lateral dynamic response of a high pier viaduct under turbulent wind during the high-speed train travel. Eng. Struct. 165, 368–385.
Premoli, A., Rocchi, D., Schito, P., Tomasini, G., 2016. Comparison between steady and moving railway vehicles subjected to crosswind by CFD analysis. J. Wind Eng. Ind. Aerod. 156, 29–40.
Rankine, W.J.M., 1882. In: A Manual of Applied Physics, tenth ed. Charles Griff and Co.
Rott, N., 1958. On the viscous core of a line vortex. Z. Für Angew. Math. Phys. ZAMP 9, 543–553.
Schober, M., Weise, M., Orellano, A., Deeg, P., Wetzel, W., 2010. Wind tunnel investigation of an ICE 3 endcar on three standard ground scenarios. J. Wind Eng. Ind. Aerod. 98, 345–352.
Sesma, I., Vinolas, J., San Emeterio, A., Gimenez, J.G., 2012. A comparison of crosswind calculations using a full vehicle and a simplified 2D model. Proc. Inst. Mech. Eng. - Part F J. Rail Rapid Transit 226, 305–317.
Sun, Z., Dai, H., Gao, H., Li, T., Song, C., 2019. Dynamic performance of high-speed train passing windbreak breach under unsteady crosswind. Veh. Syst. Dyn. 57, 408–424.
Suzuki, M., Okura, N., 2016. Study of aerodynamic forces acting on a train using a tornado simulator. Mech. Eng. Lett. 2, 1–8.
Tamura, Y., Suda, K., Yoshida, A., Matsui, M., 2007. Estimation of wind conditions around site of accident to limited express of JR Uetsu-line on December 25, 2005. Summ. Tech. Pap. Annu. Meet. Jpn. Assoc. Wind Eng. 40–41, 2007.
Thomas, D., Diedrichs, B., Berg, M., Stichel, S., 2010. Dynamics of a high-speed rail vehicle negotiating curves at unsteady crosswind. Proc. Inst. Mech. Eng. - Part F J. Rail Rapid Transit 224, 567–579.
Tomasini, G., Giappino, S., Corradi, R., 2014. Experimental investigation of the effects of embankment scenario on railway vehicle aerodynamic coefficients. J. Wind Eng. Ind. Aerod. 131, 59–71.
Wurman, J., Alexander, C.R., 2005. The 30 May 1998 Spencer, South Dakota, storm. Part II: comparison of observed damage and radar-derived winds in the tornadoes. Mon. Weather Rev. 133, 97–119.

Xu, R., Wu, F., Zhong, M., Li, X., Ding, J., 2020. Numerical investigation on the aerodynamics and dynamics of a high-speed train passing through a tornado-like vortex. J. Fluid Struct. 96, 103042.
You, W., Kwon, H., Park, J., Shin, Y., 2018. Effect of wind gusts on the dynamics of railway vehicles running on a curved track. Proc. Inst. Mech. Eng. - Part F J. Rail Rapid Transit 232, 1103–1120.
Zhai, W., Han, Z., Chen, Z., Ling, L., Zhu, S., 2019. Train–track–bridge dynamic interaction: a state-of-the-art review. Veh. Syst. Dyn. 57, 984–1027.
Zhai, W., Xia, H., Cai, C., Gao, M., Li, X., Guo, X., Zhang, N., Wang, K., 2013. High-speed train–track–bridge dynamic interactions – Part I: theoretical model and numerical simulation. Int. J. Rail Transp. 1, 3–24.
Zhang, J., Wang, J., Wang, Q., Xiong, X., Gao, G., 2018. A study of the influence of bogie cut outs' angles on the aerodynamic performance of a high-speed train. J. Wind Eng. Ind. Aerod. 175, 153–168.